LARGE-SCALE MOTIONS IN THE MARINE ATMOSPHERIC SURFACE LAYER

R. S. BOPPE, W. L. NEU and H. SHUAI
Department of Aerospace and Ocean Engineering, Virginia Polytechnic Institute and State University, Blacksburg, VA 24061, U.S.A.

(Received in final form 2 March 1999)

Abstract. Multi-level turbulent wind data from the Risø Air-Sea Experiments (RASEX) were used to examine the structure of large-scale motions in the marine atmospheric surface layer. The quadrant technique was used to identify flux events (ejections/sweeps). Ejections, which appear to occur in groups, are seen to occur first at the upper level, moving successively to lower levels with small time delays. A strong correlation between events at different heights suggests that they may all be part of a single large structure. Cross-correlation between velocity signals was used to estimate orientation of the structure using Taylor's hypothesis. The inclination of this structure is shallow ($\simeq 15°$) near the surface and increases with height. Spatial representations of the fluctuating wind vectors show a structure that is strikingly similar to conceptual models of transverse vortices and shear layers seen in laboratory flows and direct numerical simulation (DNS) of low Reynolds number flows. Spatial visualization of velocity fluctuations during other time periods and conditions clearly shows the existence of shear layers, transverse vortices, plumes, and downdrafts of various sizes and strengths. A quantitative analysis shows an increase in the frequency of shear related events with increasing wind speed.

Keywords: Coherent structures, Turbulence, Surface layer.

1. Introduction

Quasi-coherent motions in turbulent flows are a well documented phenomenon (see, e.g., Hussain, 1986; Robinson, 1991; Mahrt and Gibson, 1992). Following observations in the laboratory and visualization of data from low Reynolds number numerical simulations (e.g., Robinson, 1990; Gerz et al., 1994; Rempfer and Fasel, 1994), it is widely accepted that these structures play an important role in the mechanics of turbulent boundary layers. The intermittent nature of turbulence has also been studied in the high Reynolds number flow of the atmospheric boundary layer, focusing mainly on surface-layer turbulence. Much of the effort has been directed towards identifying extreme heat and momentum flux events in the probe data and associating them with coherent motions. Under unstable conditions, such motions have been attributed mainly to buoyancy related events such as surface-layer plumes or mixed-layer thermals (e.g., Kaimal and Businger, 1970; Kaimal, 1974; Wilczak, 1984; Williams and Hacker, 1992). However, shear related events also play an important role in the flux mechanism, particularly in near-neutral or stable

Boundary-Layer Meteorology **92:** 165–183, 1999.

conditions of the surface layer. Many studies have identified coherent structures in the surface layer over land (e.g., Katul et al., 1994; Högström and Bergström, 1996), vegetation (e.g, Collineau and Brunet, 1993; Gao et al., 1992), ice (e.g., Lykossov and Wamser, 1995) and water (e.g., Boppe and Neu, 1995). These studies have tried mainly to quantify the contribution of coherent motions to the shear stress and give an estimate of their intermittent nature in terms of frequency of occurrence. Little detail of the flow field in the vicinity of such events is known at present. The intent of this paper is to contribute to the understanding of the internal structure and three dimensional nature of coherent motions in atmospheric turbulence over water. It is hoped that as we work toward this understanding, we will gain insight into the mechanics of the surface fluxes that will be useful to fine scale modelling of these fluxes.

Techniques used to study coherent motions have varied widely, often leading to interpretations that have appeared inconsistent. Moreover, in the past, there was little consensus on the terminology used to describe the observed structures. In an effort to give the knowledge an organized form, Robinson (1990, 1991) proposed eight classes into which the various structural features were grouped, as well as possible evolution and decay mechanisms of coherent structures for low Reynolds number turbulent boundary layers.

The dominant structures in these conceptual models, which have been called ‘molecules of turbulence’, are the arch-shaped or hairpin vortical structures (Figure 1). These function as pumps to transport mass and momentum across the mean velocity gradient. Other structural features, e.g., ejections (denoted as $u'v'2$ in the figure – it is customary in engineering literature to use v for vertical velocity), sweeps ($u'v'4$ in the figure), and shear layers, are related to these vortical arches. These models provide a framework to explore the possibility of such structures being universal features of turbulent boundary layers.

Ejection and sweep motions have also been associated with sharp gradients caused by edges of large eddies. (Chen and Blackwelder, 1978; Robinson, 1990; Mahrt and Gibson, 1992; Mahrt and Howell, 1994). Such gradients have been called ‘microfronts’ in atmospheric flows (Mahrt, 1989). Figure 2 gives a schematic of a microfront and its associated motions in terms of Robinson’s hypothesis concerning the form of these structures. The microfront, referred to as a ‘back’ by Robinson (1990, 1991) is a shear layer separating regions of high speed ($+u'$) and low speed ($-u'$) fluid. Robinson hypothesized that transverse vortices, which roll up on such shear layers, may grow into vortical arches.

These vortical motions manifest themselves as a positive or negative fluctuation in the streamwise velocity, depending on where the probe is relative to the structure. Detection as well as detailed investigation of such structures is complicated by their three-dimensional nature and their large deviations in shape, size, orientation and advection velocity. Further, little is known about the growth and decay cycles of such structures at high Reynolds numbers. Thus identifying such structures in the flow is subjective. Ideally, one would like to be able to identify the structure in the

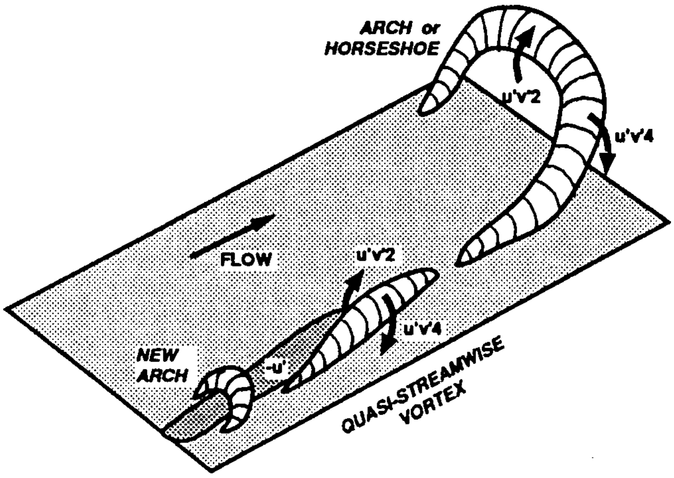

Figure 1. Schematic of arch (horseshoe) vortex and a possible regeneration mechanism for a low-Reynolds number canonical boundary layer. Also shown are kinematic relationships between ejection/sweep motions and quasi-streamwise vortices and ejection/sweeps and arch-shaped vortical structures in the 'outer' region (Robinson, 1990).

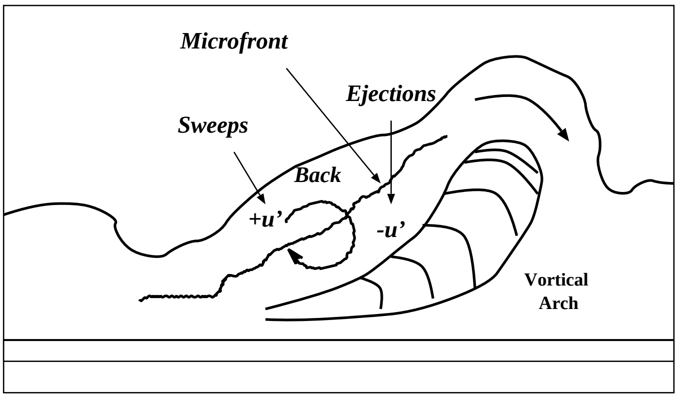

Figure 2. Schematic of eddy microfront giving rise to ejection and sweep motions. Possible rollup of new vortex on the shear layer is indicated (after Robinson, 1990).

flow and follow it in space. In order to capture details of the flow field associated with the large-scale motions, a large and dense three-dimensional sensor array is needed. Such a setup would be extremely expensive. Even then, only those structures whose configuration matches the sensor setup would be recorded with any reliability (Hussain, 1981). Alternatively, computers may one day evolve, powerful enough to simulate the high-Reynolds-number flow using direct numerical simulation. For now, given these constraints, one has to be content with the limited and partial data that are available.

Boppe and Neu (1995) describe such structures in the marine atmospheric surface layer using single-point velocity measurements. These measurements give no information on the spatial structure and orientation of the large-scale motions. The Risø data set (Barthelmie et al., 1994) alleviates this situation to a certain extent. Velocity measurements were made at multiple heights providing an opportunity to study the spatial structure (though only in one plane). This might shed light on the different sizes, orientation, and frequency of occurrence of these large-scale structures. As Boppe and Neu (1995) found little dependence of these structures on surface-wave conditions, that dependence will not be addressed in this study.

2. Data Set

The data set was collected during the course of the Risø Air-Sea Experiments (RASEX) (Barthelmie et al., 1994), which were conducted during the spring and fall of 1994 at the offshore wind farm at Vindeby in Denmark. Topography at Vindeby is flat and lies close to sea level. No topographic enhancement of wind speed is expected. Long open-sea fetch (15–25 km) occurs for wind with azimuth ranging from 225–345°. Other directions present a variety of fetches which may be used to examine fetch dependence. A long fetch may be desirable to approach fully developed wave conditions. This may help, to a certain extent, in rationalizing the assumption of a statistically stationary flow field.

The data used in the present study were collected by instruments installed on a meteorological mast which measured mean wind speed, wind direction, absolute temperature and temperature difference between levels. Six 3D fast-response sonic anemometers (Gill/Solent 3-axis ultrasonic anemometer) were used to measure vector wind speed/direction fluctuations at nominal heights of 3, 6, 10, 18, 32 and 45 m above the surface. Samples of these variables were taken at the rate of 20 Hz and stored as half-hourly time series.

The instantaneous wind vectors were averaged over an entire 30 minute record to get the mean wind vector, transformed to a coordinate system defined by the mean wind vector and expressed as $U = (u, \; v, \; w)$ where u is along the mean wind vector, v in the horizontal cross-flow direction and w in the vertical direction. Each component was then stored as a mean and fluctuating part. Another important step in data reduction was to high-pass filter the signals through a moving average filter with a cutoff at 1 minute. Small-scale turbulent motions, like ejections and sweeps, may be masked by gusts or internal gravity waves (Lykossov and Wamser, 1995). The moving-average filter removes such masking effects while preserving the small-scale motions (Boppe and Neu, 1995). The filter removed, on average, 48% of the u variance, 5% of the w variance and 20% of the momentum flux at the

10 m elevation. Estimates of atmospheric stability (in the form of z/L) have been obtained from one-hour averages of the 10-m sonic buoyancy flux.

3. Temporal Fluctuations

The first set of data files selected were during a period when the surface layer was near neutral stability but slightly stable ($z/L = 0.22$). This criteria helps in neglecting buoyancy effects during interpretations of observed structures. The initial data files are coded 131216, which indicates that the data were collected during the 13th of October, starting at 1216 hrs. The mean wind speed at 10 m above the sea was 6.37 m s^{-1}.

A time history of the fluctuating component of the streamwise velocity (u'), at different levels, is seen in the upper frame of Figure 3. As expected, the turbulence intensity (proportional to u_{rms}) decreases with height. It can be seen, during certain time intervals, that fluctuations at different levels seem to be correlated with each other, with a certain time delay. In order to accentuate these correlations, wavelet filtering (Farge, 1992) was performed. The threshold for the filter was kept high in order to see only the strong motions. The filtered signals are seen in the lower frame of Figure 3. These 'enhanced' signals facilitate the visual detection of the large organized motions. The time interval between 400 and 600 s in Figure 3 seems to have two structures which extend across the depth of the surface layer. These structures have been marked with the lines on the figure, which have been subjectively drawn, by eye, but are held constant in the following figure to serve as a reference.

The quadrant technique (Wallace et al., 1972; Lu and Willmarth, 1973) has been used to detect ejections. Bogard and Tiederman (1986) recommend a value of 1.0 for the threshold value, H, used in this method, although they demonstrate that using a value above 2.0 maximizes the probability that a detection is valid. In order to reduce the possibility of false detections, a threshold of $H = 2.0$ was used at all heights. At the higher elevations the ejections are weaker, and many may go undetected at this threshold. It is possible that decreasing the threshold with increasing height may result in detection of these weaker ejections, so as to better resolve the structure.

It is interesting to note that the ejections, seen in Figure 4, also line up well with the reference lines. Intuitively, these marked structures, which give rise to negative and then positive fluctuations in the streamwise velocity, could be associated with microfronts or 'backs' of large eddy structures (Figure 2). The second of these marked structures will be examined further in the following section.

Several authors performing quadrant technique analyses have listed the percentage contribution to total momentum flux from motions in each of the four quadrants. First through fourth quadrant motions are defined according to the signs of the streamwise and vertical velocity fluctuations, u' and w' respectively. Ejec-

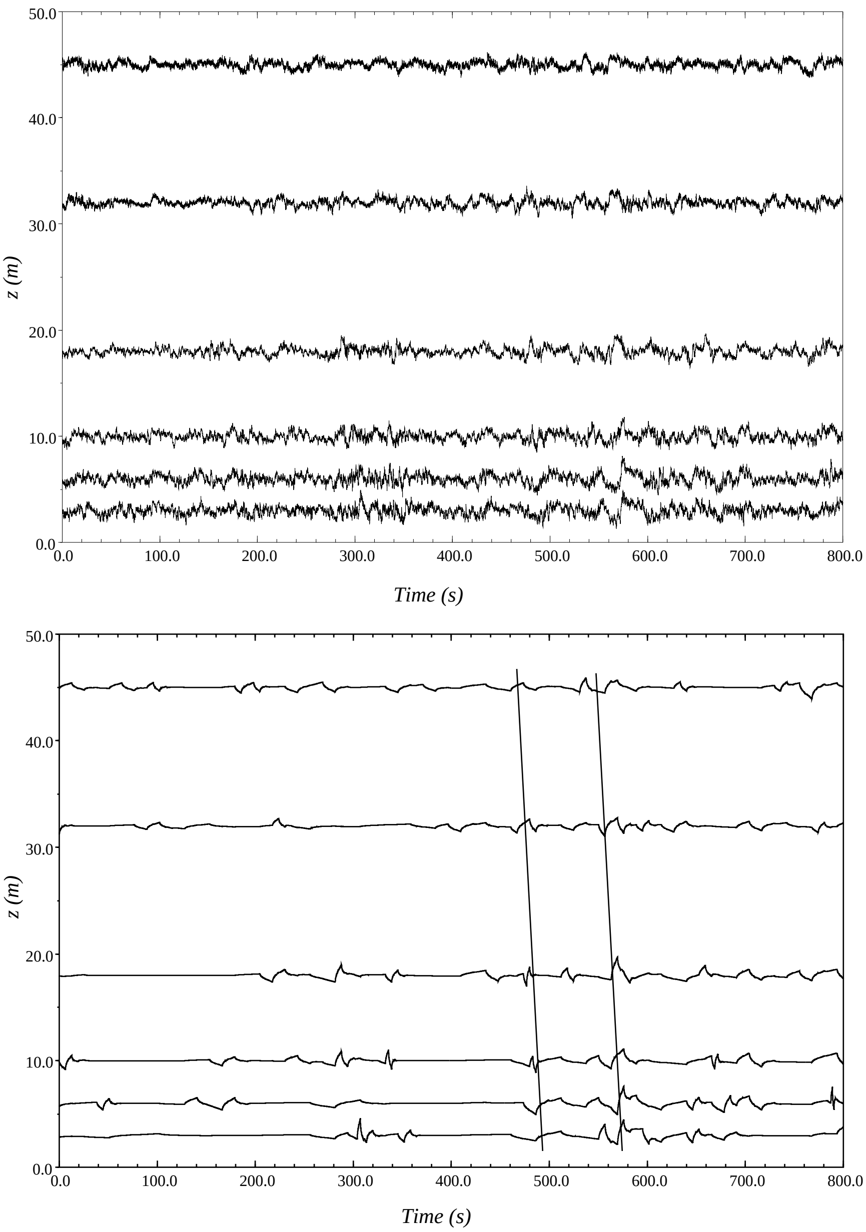

Figure 3. Upper frame: Fluctuations of streamwise velocity component, u', measured at the six anemometer heights, z. The rms fluctuation of the signal at $z = 10$ m is 0.42 m s^{-1}. Lower frame: Wavelet filtered fluctuations of streamwise velocity component.

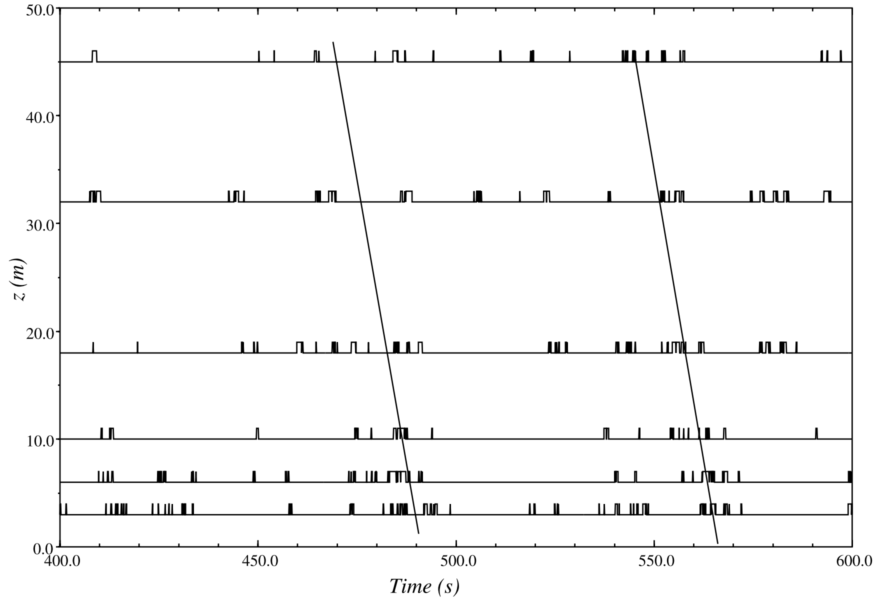

Figure 4. Timeline of ejections, detected by the quadrant technique, in the signals of Figure 3.

TABLE I

The percent contribution to the total momentum flux due to motions in each of the four quadrants at each measurement height. Numbers are averages of those obtained from the data files listed in Table II.

	1st quad.	2nd quad.	3rd quad.	4th quad.
3 m	−19	75	−20	64
6 m	−23	78	−24	68
10 m	−29	87	−30	72
18 m	−29	83	−28	74
32 m	−35	88	−33	80
45 m	−41	95	−40	85

tions are second quadrant motions ($u' < 0, w' > 0$), sweeps are fourth quadrant motions ($u' > 0, w' < 0$) and first and third quadrant motions were termed outward and inward interactions by Wallace et al. (1972). The percentages listed in Table I are very similar to those given by others which are summarized in Boppe and Neu (1995). Given are averages over the data files used in Section 4.3, as summarized in Table II, with exclusion of a few outliers. The increase in the numbers with height indicates that the coherence of the motions decreases with height.

4. Spatial Structure

A Taylor's hypothesis transformation, $x = ct$, is used to educe the spatial nature of these motions, assuming the turbulence field is frozen in time and is transported horizontally past the probe at a speed c. It is obvious that turbulence in the atmosphere is not frozen, however, it has been suggested (e.g., Stull, 1988) that the eddy life is typically long compared to the time it takes to travel across the sensor.

4.1. Orientation of the large-scale motion

The slope of the lines in Figures 3 and 4 suggests that the structures associated with these strong motions are inclined. The probes at the upper levels 'see' the structures first, then, after a time delay, the structures move past the probes at the lower levels. The time delays can be used to estimate the orientation and size/shape of these structures. Cross-correlation between the signals at the different levels is used to estimate these time delays.

Data segments of length 50 s were selected (starting from $t = 530$ s; Figure 4) for the analysis. The reference signal, assigned index 1, is the 45 m u' signal. Signals at successively lower heights have been assigned indices 2 through 6. The cross-correlation between signal 1 and signals at the other heights (viz., 32 m through 3 m), is given by,

$$R_{1j}(\tau) = \frac{\overline{u'_1(t)u'_j(t+\tau)}}{(u'_1)_{rms}(u'_j)_{rms}}$$

and is plotted in Figure 5. Curve R_{11} is the autocorrelation of the 45 m u' signal. It can be seen that peaks of the cross-correlations are shifted by positive lags. These shifts indicate how much an organized feature is lagging behind a corresponding feature at other levels and have been used to estimate the structure orientation. Unfortunately, the width of peaks 4 and 6 compromises the objectivity of the procedure. Time lags were chosen near the mid-points of these peaks.

Researchers (Kaimal, 1974; Davidson, 1974; Wilczak and Businger, 1984; Perry and Li, 1990) have found that the large-scale motions in a turbulent boundary layer advect at a speed different from the local wind speed. They have also found that the advection velocity depends on the size of the structure, the stability of the boundary layer, the distance from the surface and the surface roughness condition. However, Kaimal and Finnigan (1994) suggest that, under certain circumstances, the local mean wind, $\overline{u}$, can be used as the advection velocity of organized structures. For the present study, both the mean wind at the measurement height (local mean) and the average wind velocity across the measurement depth have been used as the advection velocities in order to estimate the orientation of the structure.

Using Taylor's hypothesis and these advection velocities, the time delays imply distances which have been plotted in Figure 6 on a 1:1 grid to give an idea of the orientation. It can be seen that for the observational height range of the

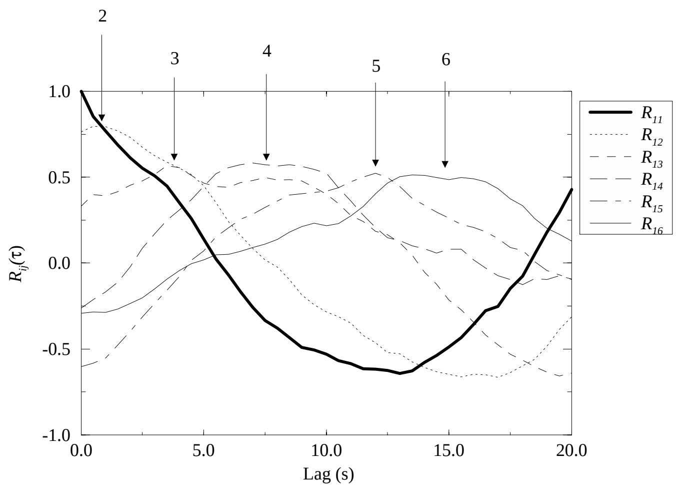

Figure 5. Cross-correlation of the u' signals at different levels.

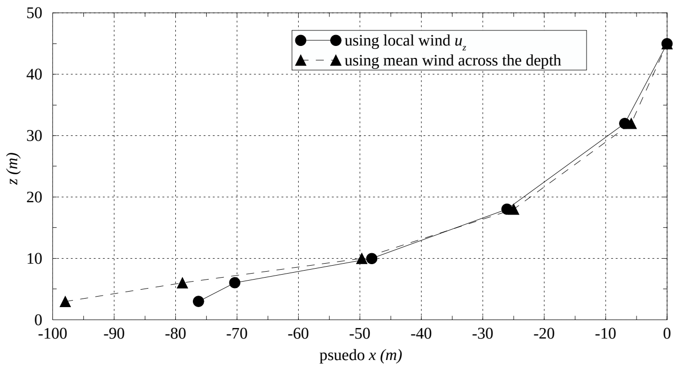

Figure 6. Spatial orientation of a large-scale motion.

experiments, the difference in advection velocity estimates has little significance. The structure seems to be inclined at an angle of about 45° above $z = 18$ m, and below that advects at very shallow angles ($\simeq$ 15°) to the surface. It should be noted that the structure may be constantly stretching and changing orientation. Also, choosing a different reference level will lead to a different orientation estimate. For comparison, Phong-anant et al. (1980) estimate inclination angles ranging from 21–47°, for temperature 'ramps' in the first 8 m of the atmospheric surface layer. Kaimal (1974) estimated angles between 35–56° with an average of 43° for convecting thermal plumes in the surface layer. Wilczak and Tillman (1980) also found similar inclination angles and curvature to their plumes. It is possible that many of the thermal signals analyzed in these studies are manifestations of the shear layers discussed below.

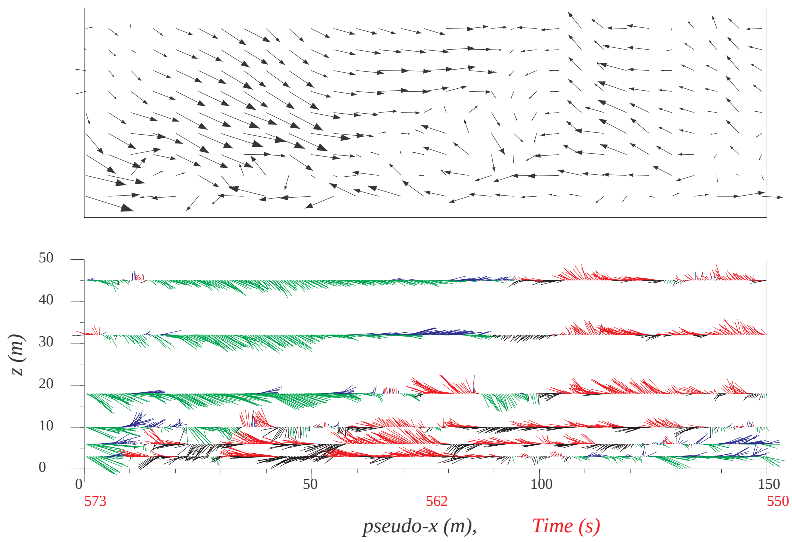

Figure 7. Velocity fluctuations (u', w') in space; shear layer associated with a vortical structure. Black labels on the abscissa are pseudo $x = \overline{u_z}t$, red labels are time from the start of the data file, increasing right to left. Wind direction is to the right. The upper frame is velocity fluctuations, low-pass filtered and interpolated to a 5 m grid. The lower frame is the data, colour coded by quadrant of fluctuation. Advection velocity, $\overline{u_z} = 6.58$ m s^{-1}.

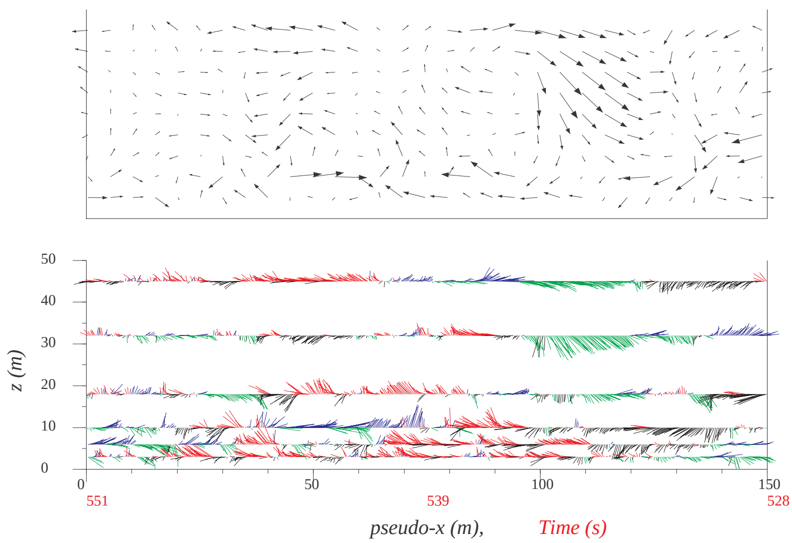

Figure 8. Velocity fluctuations in space; possible head of a vortical arch. Format as in Figure 7. Frame immediately follows Figure 7 in pseudo x (or precedes it in time).

4.2. Spatial velocity fluctuations

Figures 7 and 8 show the spatial velocity fluctuations (u', w') relative to a frame of reference moving with the average wind velocity across the measuring heights, $\overline{u_z}$ ($= 6.58$ m s^{-1}, for the current file). Here again, the 1 min. moving-average filter is applied to the data as it provides an apparent effect of the frame of reference advecting with a local wind velocity (as it should be) as opposed to a long-time-mean wind. The abscissa is a 'pseudo' distance, x, obtained by the transformation $x = \overline{u_z}t$. In the lower frame of each figure, the fluctuations have been colour coded for ease in interpretation. Colours blue, red, black and green represent the first through fourth quadrant motions on the $u'w'$ plane, respectively, i.e. red lines represent the ejection motions (second quadrant; $u' < 0, w' > 0$) and green lines represent sweeps (fourth quadrant; $u' > 0, w' < 0$). In the upper frame of the figure, the velocity fluctuations have been low-pass filtered at 2 Hz and linearly interpolated to a 5 m uniform grid. This representation makes it easier to identify shear layers and vortex motions in the fluctuation vectors.

The two figures span the time interval 528–573 s, which contains the structure that was analyzed with the cross-correlation above. Following the fluctuations in space, the 'back' of the large-scale motion, as seen in Figure 2, is quite apparent. The green, fourth-quadrant (sweep) motions are seen from 0–100 m on the pseudo x-axis of Figure 7. Red, second-quadrant (ejection) motions are seen from $x \simeq 30$ m at the lower levels in Figure 7 up to $x \simeq 20$ m in the next frame (Figure 8). A transverse vortex rolling up on this shear layer is also evident at $x \simeq 85$ m in Figure 7. Downstream (Figure 8), a large, eddy-like motion is apparent from 70–120 m. Its position relative to the shear layer suggests that it may be the 'head' of a large vortical arch (as in Figure 2). Many similar structures have been observed during other periods when wind shear was dominant in the surface layer. These observations suggest that many large-scale motions in a near-neutral atmospheric surface layer may be manifestations of transverse vortical-arch-like structures.

4.3. Spatial structure of commonly observed motions

Observations suggest the existence of vortical structures, shear layers, and plumes of various sizes and strengths. What follows is a physical description of a few of the typical structures, observed.

Figure 9 shows (u', w') velocity fluctuations during a period when the surface layer was very near neutral stability ($z/L = .024$). Wind speed at 10 m above the surface was 8.4 m s^{-1}. The fluctuations show evidence of a large transverse vortex, which extends across the measurement depth.

Figure 10 is from another near-neutral case ($z/L = -0.056$, $\overline{u_{10}} = 12.2$ m s^{-1}). The figure shows a very strong shear layer along with a transverse vortex (or two) rolling up on this shear layer. This is consistent with the model proposed by Robinson (1990), and may indeed be a universal feature of the turbulence generation mechanism.

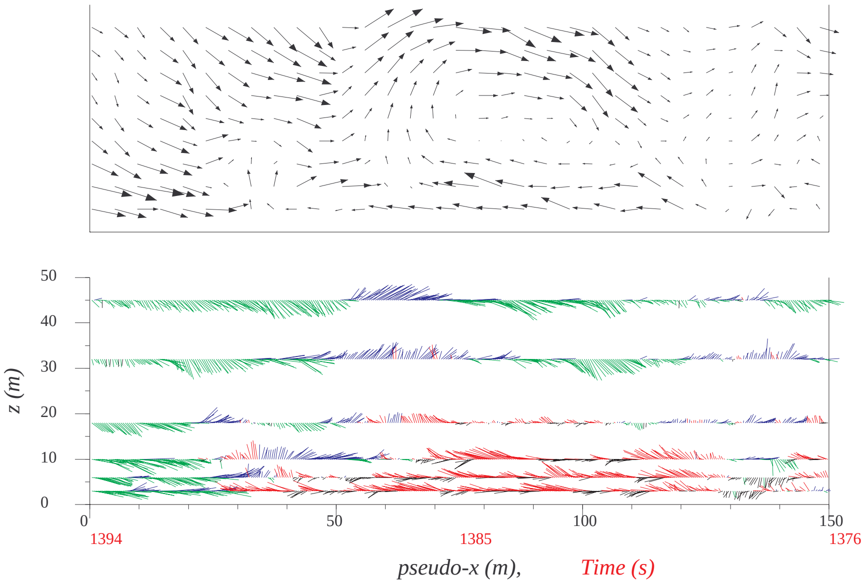

Figure 9. A typical large transverse vortex. Format as in Figure 7. Advection velocity, $\overline{u_z} = 8.3$ m s^{-1}.

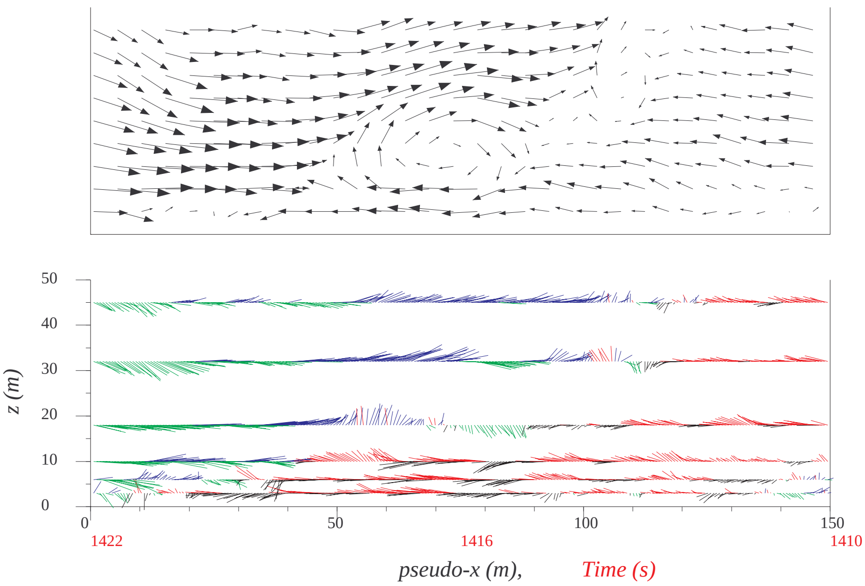

Figure 10. Strong shear layer with two transverse vortices rolling up on it. Format as in Figure 7. Advection velocity, $\overline{u_z} = 12.16$ m s^{-1}.

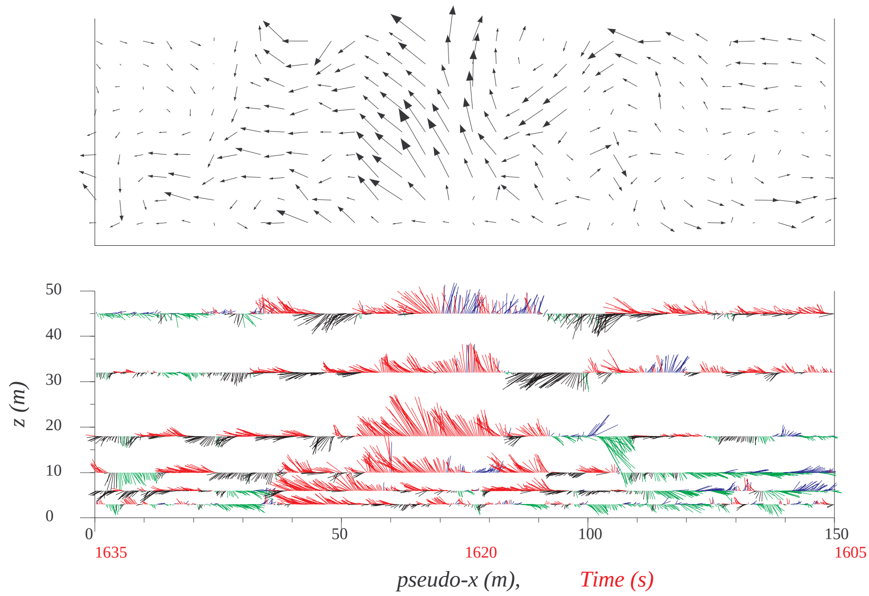

Figure 11. Surface layer plume. Format as in Figure 7. Advection velocity, $\overline{u_z} = 5.02$ m s^{-1}.

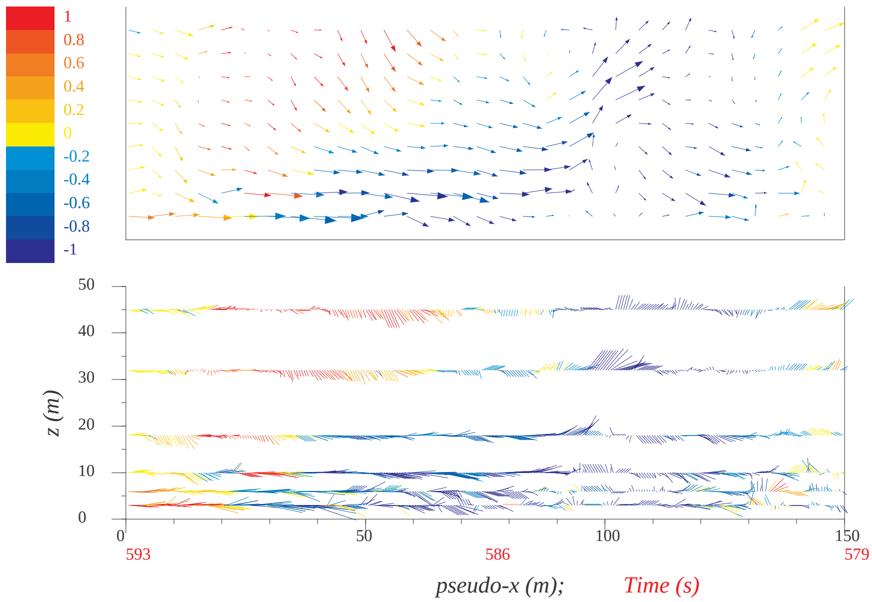

Figure 12. Velocity fluctuations colour-coded using the value of the transverse component, v'; red for $v' = 1$ m s^{-1} and blue for $v' = -1$ m s^{-1}.7 The pattern of the direction change of the transverse component suggests that this may be the leg of a vortical arch structure. Advection velocity, $\overline{u_z} = 10.76$ m s^{-1}.

A case when the surface layer was slightly more unstable, ($z/L = -0.158$, $\overline{u_{10}} = 5.2$ m s^{-1}) is shown in Figure 11. Velocity fluctuations in this figure show fluid from the near-surface region rising almost vertically. Fluctuations of this sort suggest buoyancy related effects, such as surface-layer plumes, which are easily distinguished from the shear related effects when viewed in this type of figure.

The cross-flow component (v') also shows significant correlation in several cases which may be used to speculate on the lateral position of the large-scale motion relative to the probes. Figure 12 ($z/L = 0.249$, $\overline{u_{10}} = 10.3$ m s^{-1}) shows the u' and the w' components of the flow field which are now colour-coded based on the crossflow (v') component. The colour-gradient shows a value of v' = 1 m s^{-1} for red, gradually decreasing to a value of $v' = -1$ m s^{-1} for blue. Physically, fluctuations shown in red go into the plane of the paper, and blue come out of the plane. The variation of v' seen can be interpreted as the flow rotating about an axis which has a streamwise direction and an inclination of about 45° to the surface. This flow could be due to the leg of a vortical arch structure (Figure 1) as it advects across the probes with the head of the arch passing to the right of the tower, or, from the perspective of the figure, in front of the tower. Also, in the upper right of the frame is the suggestion of the flow up and around the shoulder of the arch.

4.4. Frequencies of Observed Motions

The previous section emphasized physical description of a few commonly observed structures. An attempt has also been made to tabulate the frequency of occurrence of some common coherent motions. These statistics are based on the analysis of 27 data records (13.5 hours of data) chosen from the Spring and Fall phases of the field experiments. The data files have a wind speed (at $z = 10$ m) ranging from 4.3–12.6 m s^{-1}. Table II shows the number of occurrences of the commonly observed motions along with other parameters for each file. This tabulation is the result of a tedious and subjective frame-by-frame analysis of the listed data files. Although rules were laid down to make this quantitative analysis as objective as possible, personal judgment and bias often led to different inferences being drawn.

Table II gives the number of occurrences of ejections (Q2), sweeps (Q4), shear layers (SL), transverse vortices (TV), combination of shear layers upstream of a transverse vortex (CS), plumes (or updrafts) and downdrafts (DD), in each of the half-hour records. Ejections and sweeps were defined as second (red) and fourth (green) quadrant motions, respectively, observed without the other in the immediate neighborhood (± 25 m). The region of second or fourth quadrant motion must extend over 25 m in height and 50 m in length. Shear layers were defined as an interface between a region of red and green extending at least 25 m in height and 50 m in length. A transverse vortex was required to have a distinct vortical flow pattern in the x-z plane centered at a height of at least 10 m. If a shear layer occurred within two vortex diameters downstream of a transverse vortex, they were

TABLE II

Frequency of occurrence of ejections (Q2), sweeps (Q4), shear layers (SL), transverse vortices (TV), combination of SL and TV (CS), plumes, and downdrafts (DD) in each half-hour record, along with file ID, mean wind direction from vane at 43 m (deg.), mean wind speed at 10 m (m s^{-1}), and stability parameter z/L.

File	Wind Dir.	U_{10}	z/L	Q2	Q4	SL	TV	CS	Plumes	DD
Spring										
281412	263	7.67	0.135	1	4	9	14	1	0	0
281442	266	8.48	0.142	5	7	15	6	1	0	0
281542	267	7.78	0.140	4	7	12	7	1	0	0
281642	267	6.27	0.140	3	5	24	5	3	0	0
010022	274	12.15	−0.056	11	9	4	18	4	13	7
010122	274	12.60	−0.049	16	19	17	22	3	8	3
010152	274	12.04	−0.049	11	21	15	20	5	8	2
011105	285	9.37	−0.048	9	16	13	8	1	13	3
021307	330	6.28	−0.251	5	3	3	12	4	12	6
021337	329	5.53	−0.127	3	2	6	5	3	6	3
022107	32	4.32	−0.032	4	6	16	9	3	0	0
040007	275	8.39	0.024	8	9	1	20	3	16	8
040037	298	7.99	0.035	9	14	9	16	6	8	5
041323	195	11.21	0.249	12	10	4	16	0	0	7
041353	195	10.28	0.249	10	12	2	16	1	2	5
Fall										
131216	293	6.37	0.220	4	5	3	11	5	1	1
131246	293	6.69	0.220	8	7	4	7	1	3	0
131316	291	6.75	0.247	7	3	4	14	0	10	6
131346	274	6.24	0.195	9	4	3	14	1	3	3
131416	274	5.84	0.195	2	3	0	15	2	0	1
132346	272	6.03	−0.024	3	3	5	13	3	22	15
140316	264	5.20	−0.158	3	4	1	7	2	11	13
140416	264	6.62	−0.093	8	7	3	13	2	11	9
141710	192	3.58	−0.292	0	0	2	2	2	4	7
151552	278	5.28	0.218	2	2	3	5	2	6	7
152046	315	9.08	−0.081	5	12	12	5	4	12	10
160546	308	8.16	−0.318	10	11	7	8	5	15	14

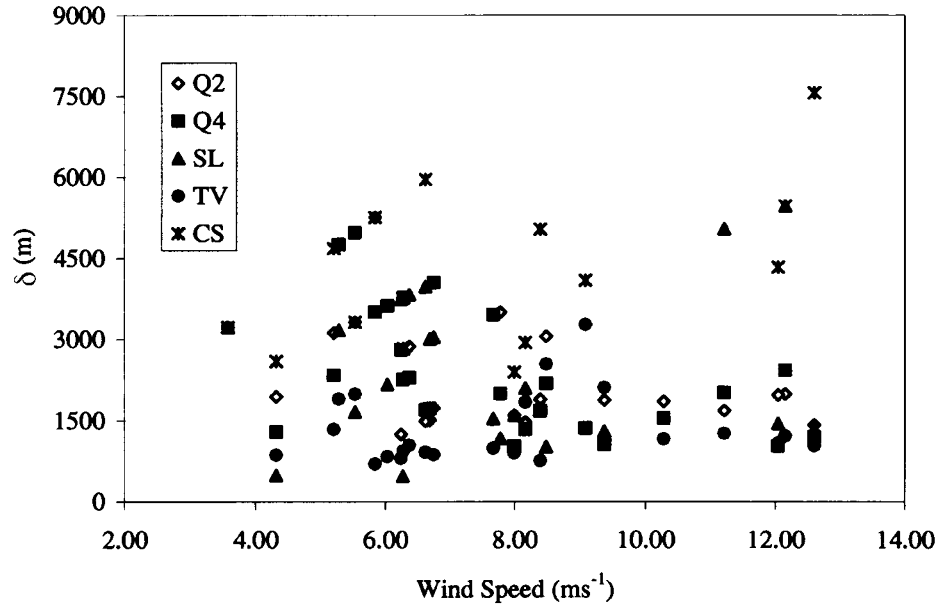

Figure 13. Mean spacing, δ, of various structures in each data file vs. wind speed.

counted as a combination structure. Plumes and downdrafts were a distinct upward or downward flow pattern covering a major portion of the measurement height range ($\simeq$ 35 m). No limit was set on the horizontal extent.

The large variability of the frequency of the events is seen here. It is apparent that the number of shear-related events (e.g., ejections, sweeps, transverse vortices) increases with increasing wind speed. It is possible that these events are equally spaced and an increasing wind speed just increases the frequency of encounter of these events with the probe. Figure 13 shows the mean spacing between the events in each data file, $\delta = 1800\overline{u_{10}}/F$, as a function of mean wind speed. F is the number of events in each 30 minute record as given in Table II. At wind speeds above about 9 m s^{-1}, the Q2, Q4 and TV motions show spacings in the relatively narrow range of 1200 – 2400 m. At lower wind speeds and for the other motions, there is no such pattern evident. Note that there are several points for which δ falls above the range of this figure. No correlation was seen between δ and z/L.

Figure 14 plots the frequency of occurrence of the buoyancy related structures (plumes and downdrafts) against the stability parameter z/L. It is expected that more of these structures will be seen with decreasing stability. As can be seen from the figure, this correlation holds only weakly. No correlation was seen between the frequency of occurrence of the buoyancy related structures and wind speed. The subjective nature of the identification of events may be partially to blame for the scatter in Figures 13 and 14.

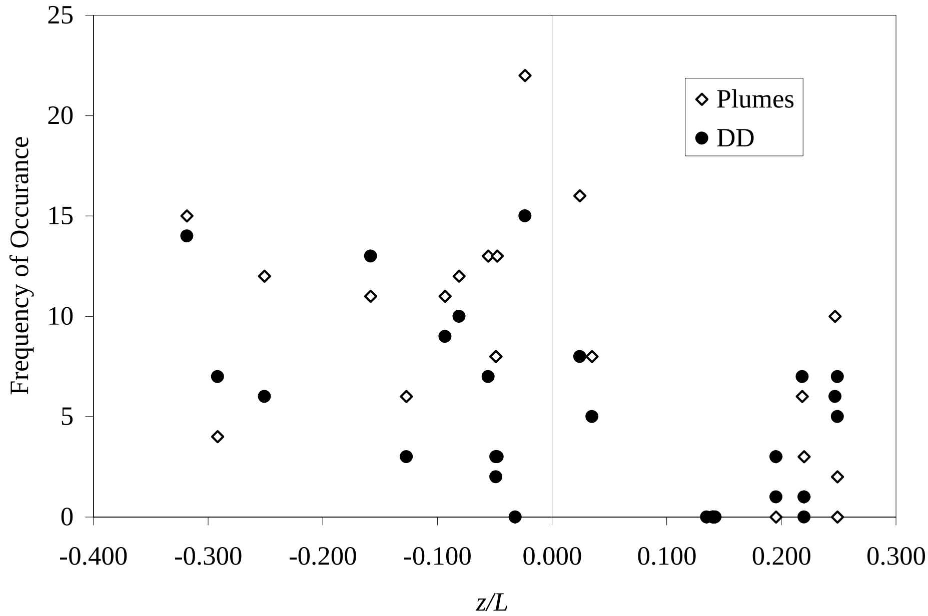

Figure 14. Frequency of occurrence of buoyancy related structures vs. z/L.

5. Conclusions

A study was conducted to reveal the spatial structure of large-scale motions in the marine atmospheric surface layer. Using velocity measurements at multiple heights, eddy-like structures of various sizes could be identified by visual observations of the velocity fluctuations. In many cases, the spatial structure has a striking resemblance to the conceptual model of a vortical arch proposed by Robinson (1990, 1991). Ejection and sweep motions are a consequence of the upstream and downstream faces of these vortical arch structures. Further, ejections and sweeps may also be due to the 'backs' (shear layers) of large transverse vortical arch like structures. These structures convect at shallow angles ($\simeq 15°$) near the surface, increasing in inclination with height and becoming much steeper above $z = 20$ m.

Apart from the vortical arch, velocity fluctuations clearly show the existence of shear layers, transverse vortices, plumes, and downdrafts in various sizes. Even though the available data give fluctuations in only one plane, the cross-flow component suggests the three-dimensional structure of the flow in many cases. Observation of 13.5 hours of data under different ambient conditions suggests an increase in the frequency of occurrence of shear-related structures with increasing wind speed and an increase in the number of buoyancy-related events with decreasing stability, though these correlations are weak.

Characterization of these structures could be used as a test bed for comparison with large-eddy or direct numerical simulations. These large-scale motions, which are qualitatively similar to their laboratory counterparts, may be a universal feature of wall-bounded turbulent shear flows.

Acknowledgements

We wish to thank Larry Mahrt and Dean Vickers for supplying the reduced buoyancy flux and mean wind direction data. This work was supported by grants N00014-93-1-0239 and N00014-96-1-0683 from the Office of Naval Research.

References

Barthelmie, R. J., Courtney, M. S., Høstrup, J., and Sanderhoff, P.: 1994, *The Vindeby Project: A Description*, Risø National Laboratory, Roskilde, Denmark, Rep. R-741(EN), 40 pp.

Bogard, D. G. and Tiederman, W.G.: 1986, 'Burst Detection with Single-Point Velocity Measurements', *J. Fluid Mech.* **162**, 389–413.

Boppe, R. S. and Neu, W. L.: 1995, 'Quasi-Coherent Structures in the Marine Atmospheric Surface Layer', *J. Geophys. Res.* **100**(C10), 20635–20648.

Chen, C. H. P. and Blackwelder, R. F.: 1978, 'Large-scale Motion in a Turbulent Boundary Layer: A Study Using Temperature Contamination', *J. Fluid Mech.* **89**, 1–31.

Collineau, S. and Brunet, Y.: 1993, 'Detection of Turbulent Coherent Motions in a Forest Canopy Part 2: Time-Scales and Conditional Averages', *Boundary-Layer Meterorol.* **66**, 49–73.

Davidson, D. S.: 1974, 'The Translation Velocity of Convective Plumes', *Quart. J. Roy. Meteorol. Soc.* **100**, 572–592.

Farge, M.: 1992, 'Wavelet Transforms and their Application to Turbulence', *Annu. Rev. Fluid Mech.* **24**, 395–457.

Gao, W., Shaw, R. H., and Paw U, K. T.: 1992, 'Conditional Analysis of Temperature and Humidity Microfronts and Ejection/Sweep Motions within and above a Deciduous Forest', *Boundary-Layer Meteorol.* **59**, 35–57.

Gerz, T., Howell, J., and Mahrt, L.: 1994, 'Vortex Structures and Microfronts', *Phys. Fluids* **6**, 1242–1251.

Högström, U. and Bergström, H.: 1996, 'Organized Turbulence Structures in the Near-Neutral Atmospheric Surface Layer', *J. Atmos. Sci.* **53**, 2452–2464.

Hussain, A. K. M. F.: 1981, 'Coherent Structures and Studies of Perturbed and Unperturbed Jets', *The Role of Coherent Structures in Modeling Turbulence and Mixing*, Springer-Verlag, New York, pp. 252–291.

Hussain, A. K. M. F.: 1986, 'Coherent Structures and Turbulence', *J. Fluid Mech.* **173**, 303–356.

Kaimal, J. C.: 1974, 'Translation Speed of Convective Plumes in the Atmospheric Surface Layer', *Quart. J. Roy. Meteorol. Soc.* **100**, 46–52.

Kaimal, J. C. and Businger, J. A.: 1970, 'Case Studies of Convective Plumes and a Dust Devil', *J. Appl. Meteorol.* **9**, 612–620.

Kaimal, J. C. and Finnigan, J. J.: 1994, *Atmospheric Boundary Layer Flows: Their Structure and Measurement*, Oxford University Press, New York, 289 pp.

Katul, G. G., Albertson, J., Parlange, M., and Stricker, H.: 1994, 'Conditional Sampling, Bursting, and the Intermittent Structure of Sensible Heat Flux', *J. Geophys. Res.* **99**(D11), 22869–22876.

Lu, S. S. and Willmarth, W. W.: 1973, 'Measurement of Structure of the Reynolds Stress in a Turbulent Boundary Layer', *J. Fluid Mech.* **60**, 481–511.

Lykossov, V. N. and Wamser, C.: 1995, ‘Turbulence Intermittency in the Atmospheric Surface Layer over Snow-Covered Sites’, *Boundary-Layer Meteorol.* **72**, 393–409.

Mahrt, L.: 1989, ‘Intermittency of Atmospheric Turbulence’, *J. Atmos. Sci.* **46**, 79–95.

Mahrt, L. and Gibson, W.:1992, ‘Flux Decomposition into Coherent Structures’, *Boundary-Layer Meteorol.* **60**, 143–168.

Mahrt, L. and Howell, J. F.: 1994, ‘The Influence of Coherent Structures and Microfronts on Scaling Laws Using Global and Local Transforms’, *J. Fluid Mech.* **260**, 247–270.

Perry, A. E. and Li, J. D.:1990, ‘Experimental Evidence for the Attached-Eddy Hypothesis in Zero Pressure Gradient Turbulent Boundary Layers’, *J. Fluid Mech.* **218**, 405–438.

Phong-anant, D., Antonia, R. A., Chambers, A. J., and Rajagopalan, S.: 1980, ‘Features of the Organized Motion in the Atmospheric Surface Layer’, *J. Geophys. Res.* **85**(C1), 424–432.

Rempfer, D. and Fasel, H. F.: 1994, ‘Evolution of Three-Dimensional Coherent Structures in a Flat-Plate Boundary Layer’, *J. Fluid Mech.* **260**, 351–375.

Robinson, S. K.: 1990, ‘A Perspective on Coherent Structures and Conceptual Models for Turbulent Boundary Layer Physics’ *AIAA 21st Fluid Dynamics, Plasma Dynamics and Lasers Conference*, Seattle, WA, *AIAA Pap. No. 90-1638*, 16 pp.

Robinson, S. K.: 1991, ‘Coherent Motions in the Turbulent Boundary Layer’, *Annu. Rev. Fluid Mech.* **23**, 601–639.

Stull, R. B.: 1988, *Introduction to Boundary Layer Meteorology*, Kluwer Academic Publishers, Norwell, Mass., 666 pp.

Wallace, J. M., Eckelmann, H., and Brodkey, R. S.: 1972, ‘The Wall Region in Turbulent Shear Flow’, *J. Fluid Mech.* **54**, 39–48.

Wilczak, J. M.: 1984, ‘Large-Scale Eddies in the Unstably Stratified Atmospheric Surface Layer. Part I: Velocity and Temperature Structure’, *J. Atmos. Sci.* **41**, 3537–3550.

Wilczak, J. M. and Businger, J. A.: 1984, ‘Large-Scale Eddies in the Unstably Stratified Atmospheric Surface Layer. Part II: Turbulent Pressure Fluctuations and the Budgets of Heat Flux, Stress and Turbulent Kinetic Energy’, *J. Atmos. Sci.* **41**, 3551–3567.

Wilczak, J. M. and Tillman, J. E.: 1980, ‘The Three-Dimensional Structure of Convection in the Atmospheric Surface Layer’, *J. Atmos. Sci.* **37**, 2424–2443.

Williams, A. G. and Hacker, J. M.: 1992, ‘The Composite Shape and Structure of Coherent Eddies in the Convective Boundary Layer’, *Boundary-Layer Meteorol.* **61**, 213–245.